Validation Process for LEWICE by Use of a Naviér-Stokes Solver

William B. Wright * Vantage Partners, LLC
Cleveland, Ohio 44135

I. Abstract

A research project is underway at NASA Glenn to produce computer software that can accurately predict ice growth for many meteorological conditions for any aircraft surface. This report will present results from the latest LEWICE release, version 3.5. This program differs from previous releases in its ability to model mixed phase and ice crystal conditions such as those encountered inside an engine. It also has expanded capability to use structured grids and a new capability to use results from unstructured grid flow solvers. An extensive comparison of the results in a quantifiable manner against the database of ice shapes that have been generated in the NASA Glenn Icing Research Tunnel (IRT) has also been performed. This paper will show the differences in ice shape between LEWICE 3.5 and experimental data. In addition, comparisons will be made between the lift and drag calculated on the ice shapes from experiment and those produced by LEWICE. This report will also provide a description of both programs. Quantitative geometric comparisons are shown for horn height, horn angle, icing limit, area and leading edge thickness. Quantitative comparisons of calculated lift and drag will also be shown. The results show that the predicted results are within the accuracy limits of the experimental data for the majority of cases.

II. Nomenclature

AOA	angle of attack (degrees)
c	chord (in)
LWC	Liquid Water content (g/m^3)
MVD	median volume diameter (μm)
T	temperature (°F)
t	time (min)

A. Subscripts

o	total

III. Introduction

The NASA Glenn Icing Branch has produced software[1-3] over the last several years for performing icing simulation in two dimensions, called LEWICE. Prior to the release of each version of LEWICE, a validation process is followed to assess the accuracy of the simulation[4-6]. While this validation process has been followed with the current version, additional validation steps are required to assess the accuracy of new capabilities. Previous validation efforts focused on the geometric comparison of ice shape features. Since the current version can produce multi-time step results using a Naviér-Stokes flow solver, comparisons can also be made to the aerodynamic degradation produced by the ice shape. Ideally, this validation would involve a comparison of the calculated lift and drag values against experimental data for lift and drag. Given the large number of icing conditions available, this is not feasible. Instead, the validation performed in this report consists of calculating the flow field on the ice shape produced from the experiment and the lift and drag values for those results are compared to the calculated lift and drag values produced by the ice shape calculated by LEWICE.

There have been a large number of papers in recent years that predict ice accretions using Naviér-Stokes flow solvers[7-34], but comparisons are typically limited to a small number of cases. Frequently, a comparison is made to a NACA0012 shape with the following conditions: c = 21 in., V =130 kts, T_o = 28°F, AOA = 4°, LWC = 1 g/m^3, MVD = 20 μm. However, the comparison is only shown for one of the Icing Research Tunnel (IRT) ice shapes ran using this condition. In fact, this case is one of the most frequently repeated icing conditions as it is part of a calibration test used to confirm that the IRT produces similar ice shapes over time. There are 46 ice shape tracings for this condition, including off-centerline tracings. Given the large number of cases, a more proper comparison would show the prediction as compared to the variability of the experiment as shown in Fig. 1. This figure shows the average of the 46 profiles along with the maximum and minimum ice shape as determined by the upper horn height. It should also be noted that since this is a very warm glaze condition, the experimental repeatability in the IRT is not as good as the repeatability for many other cases. This comparison also shows that the LEWICE prediction falls within the experimental variability. As such, no ice accretion program can claim to be better than this result. It is therefore desirable to find cases that would properly test the capabilities of ice accretion software. The current study selects 107 conditions that produce large glaze and large mixed ice shapes for evaluation. Previous comparisons have been made using Naviér-Stokes solvers with LEWICE[35-37] but this is the first comprehensive comparison involving a large number of conditions and to apply the AIAA standard for verification and validation[38].

The remainder of this report is divided into four sections. Section IV, A will cover the updates to this version of LEWICE. Section IV, B will provide a description of the Naviér-Stokes flow solver SU2[39] that was used for this effort, the grid generation software Pointwise, and the python scripts that manage the time stepping process. Section V will describe the experimental data and the parameters used for quantifying the comparisons. Section VI will provide validation results along with a statistical comparison of those parameters with the available experimental data.

IV. Existing Computational Tools

A. LEWICE

The computer program, LEWICE, embodies an analytical ice accretion model that evaluates the thermodynamics of the freezing process that occur when supercooled droplets impinge on a body. The atmospheric parameters of temperature, pressure, and velocity, and the meteorological parameters of liquid water content (LWC), droplet diameter, and relative humidity are specified and used to determine the shape of the ice accretion. The surface of the clean (un-iced) geometry is defined by segments joining a set of discrete body coordinates. The software consists of four major modules. They are 1) the flow field calculation, 2) the particle trajectory and impingement calculation, 3) the thermodynamic and ice growth calculation, and 4) the modification of the current geometry by addition of the ice growth.

LEWICE applies a time-stepping procedure to "grow" the ice accretion. Initially, the flow field and droplet impingement characteristics are determined for the clean geometry. The ice growth rate on each segment defining the surface is then determined by applying the thermodynamic model. When a time increment is specified, this growth rate can be transformed into an ice thickness and the body coordinates are adjusted to account for the accreted ice. This procedure is repeated, beginning with the calculation of the flow field about the iced geometry, then continued until the desired icing time has been reached. The results shown in this report are from version 3.5 of LEWICE. This version is not yet available for release. LEWICE 3.5 is currently under review for release and an official version will be made available upon completion of all internal review processes.

There are two major updates that pertain to LEWICE 3.5. First a capability was added to model mixed phase and ice crystal conditions such as those existing in engines. This modification consists of three sub-models. First, there are the modifications to the particle trajectory routine that track the energy transfer to and from a particle. Second, there is a model for mass loss due to erosion in a mixed phase environment. Finally, there are changes to the mass and energy balance whereby the incoming ice particles can add to the ice mass at the surface. A report on those capabilities was published last year[40] and will not be repeated in this report.

The second major modification was to expand the type of grids that could be handled by LEWICE. In the previous release, only single block structured grids could be used for single body geometries. Multi-block chimera grids could be used when analyzing multi-element airfoils. The current version can use unstructured grid input as well as multi-block structured grids including chimera grids and Cartesian grids. However, in order to use LEWICE in an automated fashion similar to the process used for potential flow solvers, a python script was created in order to manage the process. In this case, the script calls the grid generator which in this case was Pointwise[41] using the glyph scripting language[42]. Once the grid is generated, the script calls the SU2 solver to calculate the flow field. The grid and flow solver files are converted to a form that LEWICE can use with a utility program called catersian.exe. This process is similar to the process used by LEWICE3D to convert various grids and flow solutions to a format supported by LEWICE3D[43]. Once the grid and flow solutions are in a usable format, then LEWICE is run in single time step mode to produce an interim ice shape. Then the process is repeated for the

number of time steps needed. The number of time steps used by the python script is determined by the same formula used in LEWICE for calculating automated time steps when using the potential flow solver. While this process can be used to automatically calculate ice shapes using a Naviér-Stokes solver, the number of cases considered would have to be reduced. The results shown in this paper use ice shapes generated by LEWICE with potential flow and then calculation of the flow field of the final ice shape was performed using Navier-Stokes. Some ice shapes were generated using the Navier-Stokes approach and the ice shapes calculated were close to the potential flow results. However, there was insufficient time to complete the full set of cases for this paper. Because of this, the results shown in this report cannot be considered a validation of the modifications described above. Rather, this paper verifies that the changes made to this version of the code have maintained the capability of LEWICE 3.5 to produce results consistent with previous versions using the standard ice growth routines. Subsequent studies may examine the ability of the Navier-Stokes routines within LEWICE 3.5 to produce ice shapes.

B. SU2 and Grid Generation

The SU2 suite is an open-source collection of C++ based software tools for performing Partial Differential Equation (PDE) analysis and solving PDE constrained optimization problems. The toolset is designed with computational fluid dynamics and aerodynamic shape optimization in mind, but is extensible to treat arbitrary sets of governing equations such as potential flow, elasticity, electrodynamics, chemically reacting flows, and many others. SU2 is under active development by the Aerospace Design Lab (ADL) of the Department of Aeronautics and Astronautics at Stanford University and many members of the community, and is released under an open-source license. This software was chosen because it was open source and available to all users. It was also found to be a very robust solver, capable of handling iced airfoils. Their web page also had examples demonstrating how to use the glyph scripting language in Pointwise to automate the process, which was a necessary step for multi-time step ice accretion. This study used version 4.0 of the software.

Grids were generated for airfoils and ice shapes using the commercial software Pointwise. This software was chosen because it could create the variety of grids necessary for testing the capabilities of LEWICE but also because of its ease of use and amenability to automated scripting. The user interface for Pointwise was built using the Glyph2 scripting language. Glyph2 is an extension to the tcl programming language[44] that allows access to the commands and entities of the Pointwise application. Unstructured grids were used in this report, as this would allow for a better quality mesh for complex ice shapes. Previously, a system for automating a single LEWICE run using a single block structured grid was developed[36]. While this process worked well for many conditions, for large ice shapes the grids generated could become warped, leading to less accurate flow solutions. For this study, rectangular elements were used near the surface of the geometry, with triangular elements further away. This was accomplished by using a feature in Pointwise called T-rex[45]. This allowed for the specification of a y^+ of 1 at the wall. The T-rex layer was specified as being twenty cells thick, although this could be changed if it were found to be necessary. The outer grid was an O-grid placed 200 chord lengths from the airfoil. The procedure used for this study was to identify 20 cases for use in a grid resolution study. Once it was determined that the grids for these was sufficiently resolved. The refined spacing was used for the remainder of the cases.

V. Experimental Data

The experimental data described in this paper are the result of a wide variety of tests performed in the NASA Icing Research Tunnel (IRT) over the last twenty-five years. This database had been reported on previously, so only a summary of the data is presented in this report. The complete database consists of eight airfoils. These airfoils and the accompanying ice shapes represent the complete set of publicly available data that has been generated in the IRT and digitized for single element airfoils. There are a total of 1898 IRT conditions available to be analyzed for this validation report. Including repeated conditions and off-centerline tracings, there are well over 3000 experimental ice shapes to be used for validation.

The data was taken in the IRT by making an approximately ¼ inch cut in the ice growth, inserting a cardboard template into the cut and tracing the contour of the ice shape onto the cardboard template with a pencil. The pencil tracing was then transformed into digital coordinates with a hand-held digitizer. A flatbed scanner with digitizing software was available to accelerate the data acquisition process. For any given IRT test run, up to five span-wise sections of the ice shape were traced and digitized in this manner. There are several steps within this process that can potentially cause experimental error. Those that can be quantified by the current technique are the span-wise variability, the repeatability error, and errors involved in the tracing technique.

The complete database could not be analyzed with the Naviér-Stokes solver due to time constraints. Therefore a subset of this data was used. The cases selected were for conditions where the accumulation parameter based on the leading edge

diameter was greater than 3.0 and the calculated stagnation point freezing fraction was less than 0.6. This limits the study to large ice shapes with mixed or glaze icing conditions. There were 105 conditions that met these two criteria. Five of these cases are Super-cooled Large Droplet (SLD) conditions. In addition, two cases were added from the NLF0414 database to the validation list, as there existed experimental flow measurements on those ice shapes from Addy[46]. For some of these conditions, there existed repeat runs and tracings at off-centerline conditions. This finally produced a total of 171 experimental ice shapes from six airfoils to be considered in this process. The complete list of conditions is shown in Appendix A.

The six airfoils are as follows: 1) a NACA 23012, a Large Transport Horizontal Stabilizer (LTHS), a business jet airfoil, a NACA 0012, a NACA 0015, and a NLF 0414 laminar flow general aviation wing. The airfoils are shown in Fig. 2. If more than one chord size was used for an airfoil, the profile for the 36 in. chord was shown in the figure. Many of these models were described in an earlier report on the LEWICE 2.0 validation effort[5]. The complete set of conditions can be analyzed using LEWICE with a potential flow solver. The flow over the 171 tracings was calculated using the SU2 solver. For those runs, the airspeed from the icing conditions was used but the angle of attack was set at 6° to provide consistency among the cases. It was originally planned that angles of attack up to stall would be calculated, but this proved too time consuming for the number of cases considered.

VI. Results and Comparison Methodology

This section describes the methodology used to make the quantitative measurements on experimental and predicted ice shapes. This methodology has been incorporated into a software utility called THICK that calculates and outputs the parameters described. This software was created in order to process large numbers of ice shapes such as those presented in this report. This program reads two geometry files: one for the clean airfoil and one containing an ice shape. This utility has been documented more thoroughly in the LEWICE 3.0 User Manual[3]. This software has recently been revised to more accurately capture ice features of interest. An additional output file called "ReducedPeaks.dat" provides the location of other ice features that may or may not be ice horns that can be evaluated by the user. This file supplements the output "Peaks.dat" which often had too many peaks for a user to manually consider when applied to experimental ice shapes. The ice shapes are categorized using icing limit, area, horn height, horn thickness and leading edge thickness. The parameters were defined in the previous validation report[5].

The comparison methodology of geometric features will follow previous LEWICE validation efforts. Measured values are the lower and upper icing limit, area, leading edge minimum thickness, lower and upper horn thicknesses and lower and upper ice horns. The comparison for icing limit is shown in Fig. 3. The black lines within the colored bars show the upper and lower maxima of the values. This comparison shows a larger variation of the computed results compared to the variation in the experimental data. For the experimental ice shapes, the large horns tend to prevent impingement downstream. This shows that it may be necessary to run smaller time steps for the LEWICE cases to try to capture this effect. The range of variability in the upper icing limit is especially small for the experimental ice shapes. The variability of the upper icing limit for this subset of data is less than 0.5% chord as compared to an experimental variability of 4.4% for the full database as reported in previous validation reports. Since the ice shapes considered in this study are large, there are fewer repeat conditions, which can influence the calculated statistics. It should also be noted that the variability of the LEWICE comparison is also better for the reduced data set than for the full database although the difference between the experimental variability and the LEWICE comparison increased. Figure 4 shows a LEWICE result that is close to the average variability of icing limits.

Figure 5 shows the comparison for the Leading Edge Minimum Thickness and Ice Area. Once again, the experimental variability has been reduced significantly from the variability of the full database. For the full database, the experimental variability was 8.6% for the leading edge thickness and 10.3% for the area as compared to 0.8% and 1.9% respectively for the large ice shapes. This could indicate that there is induced error in measuring small experimental ice shapes while the larger ice shapes are easier to measure and are therefore more consistent. The variability of LEWICE predictions also improved from the results for the full database. The LEWICE variation was 3% for the leading edge thickness for the large glaze cases as compared to 10.4% for the full database. The LEWICE variation was 5.1% for area as compared to 16.6% for the full database. As previously mentioned, the large ice shapes have more consistent measurements and there are fewer repeats. Figure 6 shows a LEWICE result that is close to the average variability for Leading Edge Thickness and Ice Area.

Figure 7 shows the comparison for the lower and upper ice horns while Fig. 8 shows the comparison for lower and upper horn angle. The variability of the experimental horn heights is less than 2% for both the upper and lower horn heights while the comparison of LEWICE to the experimental data is approximately 6% for both. Once again, both values are significantly lower than values measured from the full database. For the horn angles, the experimental variability was 4.5° for the lower horn and 6° for the upper horn. The LEWICE variability was 21° for the lower horn angle and 16° for the upper horn angle.

The values for the LEWICE comparison are lower than the variability for the full database but are consistent with the results reported previously. The variability of the experimental results has once again improved by selecting only the largest ice shapes. There is an additional factor to consider here, however. For the reduced data set, it was possible to verify that the THICK utility selected the icing horn that a person would select if performing this task manually. With the complete database, it is likely that some of the experimental variability occurs because there were too many results to be manually verified. Since the LEWICE ice shapes are smoother, there is less chance for the THICK utility to pick poor values for the horn values. Figure 9 shows a LEWICE result that is close to the average variability for the two horn heights. Figures 10 and 11 show the average variability in the LEWICE result for Lower Horn angle and Upper Horn Angle, respectively. In both cases, the measured differences illustrate that the differences are as much a result of the THICK measurement process as they are a true difference in horn angle. Since previous studies have shown that aero performance losses for large glaze shapes are mostly a function of horn angle, it is useful to show those results as well. Figures 12 and 13 show the worst comparison based on Lower Horn Angle and Upper Horn Angle, respectively. Both predictions might be improved by using a Naviér-Stokes solver instead, but those codes must also show that they can predict the other cases as well.

As described previously, the 171 tracings from IRT experiments and the 107 LEWICE potential flow based ice shape predictions were run with the python script to get the flow solutions for the final geometries at an angle of attack of 6° using the SU2 Naviér-Stokes solver at an angle of attack of 6°. The compilation of statistics is incomplete however since many cases failed to converge. For the 171 ice shape tracings, 95 of the cases have converged solutions while for the LEWICE shapes only 52 of the conditions produced converged flow solutions. By combining these two results, it was discovered that 64 tracings provided a converged flow solution for both the tracing and LEWICE results. This occurs since some of the conditions for which the LEWICE computed ice shape has a converged solution, had multiple experimental shapes with converged solutions. In this report, both results from the flow solutions on the experimental ice shapes and the results from the flow solutions on the LEWICE ice shapes are given, but the averages cannot be compared to each other since they do not describe the same sets of data. Results from the CFD analysis of the experimental ice shapes showed that for a given icing condition, the lift coefficient for a given shape had an average difference of 0.0052 from the average of the lift coefficients for all ice shapes produced by that condition. Similarly, the CFD analysis showed that for a given icing condition, the drag coefficient for a given shape had an average difference of 0.008 from the average of the drag coefficients for all ice shapes produced by that condition. This is better illustrated by the results listed in Table 1. For case HD1075736, the lift coefficient was calculated to be 0.5996. The average lift prediction for the three shapes with that condition that had a converged flow solution (i.e. HD1075636, HD1075736, and HD1075936) was 0.6094 so the difference in lift for that case was 0.0098. The three ice shapes are shown in Figs 14-16. The Mach number contours for these three cases are shown in Figs. 17-19 and the Mach contours for the LEWICE shape are shown in Fig. 20. The surface pressure coefficients are shown in Figure 21. For the LEWICE generated ice shapes, the differences in lift and drag were calculated from each individual case rather than the experimental average for all the conditions since there were so few cases where both sets of outputs had converged solutions. The differences for each individual icing condition were then averaged, yielding an overall difference in lift prediction of 0.0159 and an overall difference in drag of 0.0249. Expressed as a percentage difference, the flow results on the LEWICE shapes were 2.9% for lift and 23.8% for drag compared to the average experimental value.

VII. Conclusions

A new version of LEWICE has been created for predicting ice accretion on 2D geometries that adds the ability to model mixed phase and ice crystal conditions such as those encountered inside an engine. It also has expanded capability to use structured grids and a new capability to use results from unstructured flow solvers. The software keeps many of the same features as LEWICE and produces similar results as previous versions for the cases compared thus far. A comparison with 2D experimental ice shape tracings confirms the fidelity of the new model. Geometric comparisons showed that while the average LEWICE comparison was larger than the experimental variation, this is due to the high fidelity of the experimental results rather than an indictment of the LEWICE comparisons.

VIII. Acknowledgements

The author would like to acknowledge the continued financial support from NASA Glenn for this research.

IX. References

1. Wright., W. B., “User Manual for the NASA Glenn Ice Accretion Code LEWICE Version 2.0”, NASA CR-1999-209409, Dec. 1999.

2. Wright, W. B., “User Manual for the NASA Glenn Ice Accretion Code LEWICE Version 2.2.2, NASA CR-2002-211723, Aug. 2002.

3. Wright, W. B., “User’s Manual for LEWICE 3.2”, NACA CR-2008-214255, Nov. 2008.

4. Wright, W. B. and Rutkowski, A., “Validation Results for LEWICE 2.0,” NASA CR 208690, Nov. 1998.

5. Wright, W. B., “Validation Methods and Results for a Two-Dimensional Ice Accretion Code,: J. of Aircraft, Vol. 35, No, 5, Sept. 1999.

6. Wright, W. B., "Validation Results for LEWICE 3.0", AIAA 2005-1243, Jan. 2005.

7. Brahimi, M T; Tran, P; Tezok, F; Paraschivoiu, I, “Numerical simulation of in-flight aircraft icing”’ ICAS, Congress, 20th, Naples, Italy, Proceedings. Vol. 2; UNITED STATES; 8-13 Sept. 1996. pp. 1522-1532. 1996.

8. Myers, T. G. and Hammond, D. W., “Ice and Water Film Growth from Incoming Supercooled Droplets”, Intl. J. of Heat and Mass Transfer, vol. 42, pp. 2233-2242, 1999.

9. Myers, T. G., Charpin, J. P. F., and Chapman, S. J., “The Flow and Solidification of a Thin Fluid Film on an Arbitrary Three-dimensional Surface”, Phys. Of Fluids, Vol. 14, No. 8, pp. 2788-2804, Aug. 2002.

10. Bourgault, Y., Boutanios, Z. Habashi, W., “FENSAP-ICE's Three-Dimensional In-Flight Ice Accretion Module, ICE3D”, Journal of Aircraft, vol.37 no.1 (95-103) 2000.

11. Beaugendre, H; Morency, F; Habashi, W G, “FENSAP-ICE's three-dimensional in-flight ice accretion module: ICE3D”, Journal of Aircraft. Vol. 40, no. 2, pp. 239-247. Mar.-Apr. 2003

12. Emmanuel, M., et al. (2009). ECLIPPS: 1. Three-Dimensional CFD Prediction of the Ice Accretion. 1st AIAA Atmospheric and Space Environments Conference, American Institute of Aeronautics and Astronautics.

13. Petrosino, F., et al. (2009). "Ice Accretion Model on Multi-Element Airfoil." Journal of Aircraft 48(6): 1913-1920.

14. Shen, X., et al. (2009). "Three-Dimensional Numerical Simulation of Ice Accretion at the Engine Inlet." Journal of Aircraft 50(2): 635-642.

15. Guy, F., et al. (2009). CIRAAMIL Ice Accretion Code Improvements. 1st AIAA Atmospheric and Space Environments Conference, American Institute of Aeronautics and Astronautics.

16. Zhihong, Z., et al. (2010). Icing Numerical Simulation for Single and Multi-Element Airfoils. 28th AIAA Applied Aerodynamics Conference, American Institute of Aeronautics and Astronautics.

17. Michael, K., et al. (2010). A Finite-Volume Approach to Modeling Ice Accretion. 28th AIAA Applied Aerodynamics Conference, American Institute of Aeronautics and Astronautics.

18. Nakakita, K., et al. (2012). "Toward Real-Time Aero-Icing Simulation of Complete Aircraft via FENSAP-ICE." Journal of Aircraft 47(1): 96-109.

19. Hasanzadeh, K., et al. (2012). "Quasi-Steady Convergence of Multistep Navier–Stokes Icing Simulations." Journal of Aircraft 50(4): 1261-1274

20. Kazem Hasanzadeh, L., et al. (2013). Validation and Verification of Multi-Steps Icing Calculation Using CANICE2D-NS Code. 31st AIAA Applied Aerodynamics Conference, American Institute of Aeronautics and Astronautics.

21. Jason, G. (2012). Computational 3-D Icing Results for Scaled DLR-F6 Geometry. AIAA Atmospheric Flight Mechanics Conference, American Institute of Aeronautics and Astronautics.

22. Weiliang, K. and L. Hong (2012). An Ice Accretion Model for Aircraft Icing Based on Supercooled Icing: Theory and Application. 50th AIAA Aerospace Sciences Meeting including the New Horizons Forum and Aerospace Exposition, American Institute of Aeronautics and Astronautics.

23. Thomas, R., et al. (2013). FENSAP-ICE Simulation of Icing on Wind Turbine Blades, Part 1: Performance Degradation. 51st AIAA Aerospace Sciences Meeting including the New Horizons Forum and Aerospace Exposition, American Institute of Aeronautics and Astronautics.

24. Andrew, P., et al. (2014). A 3D Mesh Deformation Technique for Irregular In-flight Ice Accretion Shapes. 44th AIAA Fluid Dynamics Conference, American Institute of Aeronautics and Astronautics.

25. Cao, Y. and J. Huang (2014). "New Method for Direct Numerical Simulation of Three-Dimensional Ice Accretion." Journal of Aircraft 52(2): 650-659.

26. Carlos Gallego, C. and P. R.-C. Luis (2014). Prediction of ice accretion on the nacelle of a turboprop aircraft. 52nd Aerospace Sciences Meeting, American Institute of Aeronautics and Astronautics.

27. Daniel, M. K., et al. (2014). Numerical investigation of ice particle accretion on heated surfaces with application to aircraft engines. 11th AIAA/ASME Joint Thermophysics and Heat Transfer Conference, American Institute of Aeronautics and Astronautics.

28. David, S., et al. (2014). FENSAP-ICE Simulation of Complex Wind Turbine Icing Events, and Comparison to Observed Performance Data. 32nd ASME Wind Energy Symposium, American Institute of Aeronautics and Astronautics.

29. Pierre, T. and V. Philippe (2014). Heat and mass transfer analogies for evaporation models at high evaporation rate. 6th AIAA Atmospheric and Space Environments Conference, American Institute of Aeronautics and Astronautics

30. Xiaoling, T., et al. (2014). Robust Surface Evolution and Mesh Deformation for Three Dimensional Aircraft Icing Applications on a Swept GLC-305 Airfoil. 6th AIAA Atmospheric and Space Environments Conference, American Institute of Aeronautics and Astronautics.

31. Giulio, G., et al. (2015). A model for in-flight ice accretion based on the exact solution of the unsteady Stefan problem. 7th AIAA Atmospheric and Space Environments Conference, American Institute of Aeronautics and Astronautics.

32. Lakshmi, N. S. and A. Muhammad (2015). In-Cloud Ice Accretion Modeling on Wind Turbine Blades Using an Extended Messinger Model. 13th International Energy Conversion Engineering Conference, American Institute of Aeronautics and Astronautics.

33. Marie, C. P., et al. (2015). Development of CFD-based icing model for wind turbines: A case study of ice sensor. 33rd Wind Energy Symposium, American Institute of Aeronautics and Astronautics.

34. Simon, B.-C. and L. Eric (2015). Two-Dimensional/Infinite Swept Wing Ice Accretion Model. 53rd AIAA Aerospace Sciences Meeting, American Institute of Aeronautics and Astronautics.

35. Wright, W. B. and Chung, J., "Correlation Between Geometric Similarity of Ice Shapes and the Resulting Aerodynamic Performance Degradation – A Preliminary Investigation Using WIND, AIAA-2000-0097.

36. Thompson, D. S. and Soni, B. K., "ICEG2D: A Software Package for Ice Accretion Prediction," AIAA 2003-1070, Jan. 2003.

37. Kreeger, R. and Wright, W. B., "The Influence of Viscous Effects on Ice Accretion Prediction and Airfoil Performance Predictions", AIAA-2005-1373, Jan. 2005.

38. " Guide for the Verification and Validation of Computational Fluid Dynamics Simulation", AIAA G-077-1998, 2002.

39. F. Palacios, T. D. Economon, A. C. Aranake, S. R. Copeland, A. K. Lonkar, T. W. Lukaczyk, D. E. Manosalvas, K. R. Naik, A. S. Padron, B. Tracey, A. Variyar, and J. J. Alonso, *"Stanford University Unstructured (SU2): Open-source analysis and design technology for turbulent flows*", AIAA Paper 2014-0243.

40. Wright, W., Struk, P., Bartkus, T., and Addy, G., "Recent Advances in the LEWICE Icing Model," SAE Technical Paper 2015-01-2094, 2015, doi:10.4271/2015-01-2094.

41. Steinbrenner, J. P., Michal, T., Abelanet, J.P., "An Industry Specification for Mesh Generation Software", AIAA-2005-5239, June 2005.

42. Pointwise, Software Package, Vers. 17.3 R5, Pointwise, Inc., Fort Worth, Texas, 2016.

43. Bidwell, C. S., "Icing Analysis of a Swept NACA0012 Wing Using LEWICE3D Version 3.48", AIAA-2014-2200, June 2014.

44. Tcl, Open Source Software Package, Vers. 8.5, Tcl Developer Exchange, www.tcl.tk, 2016.

45. Steinbrenner, J. P., "Construction of Prism and Hex Layers from Anisotropic Tetrahedra", AIAA-2015-2296, June 2015.

46. Addy, H. E., Broeren, A. P., Zoeckler, J. G., and S. Lee, "Wind Tunnel Study of the Icing Effects on a Business Jet Airfoil, AIAA-2003-727, Jan. 2003.

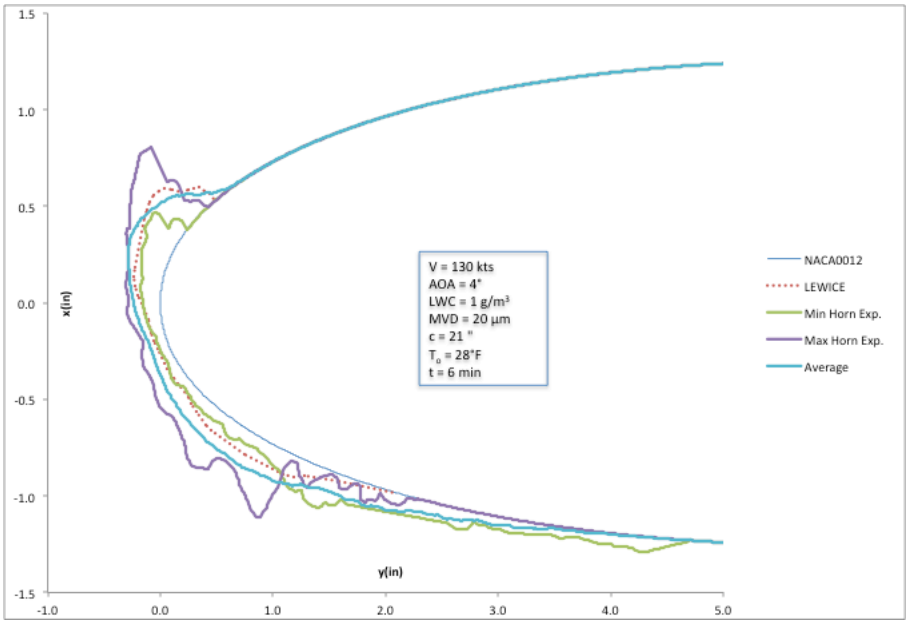

Figure 1: Ice Shape Comparison on Calibration Condition

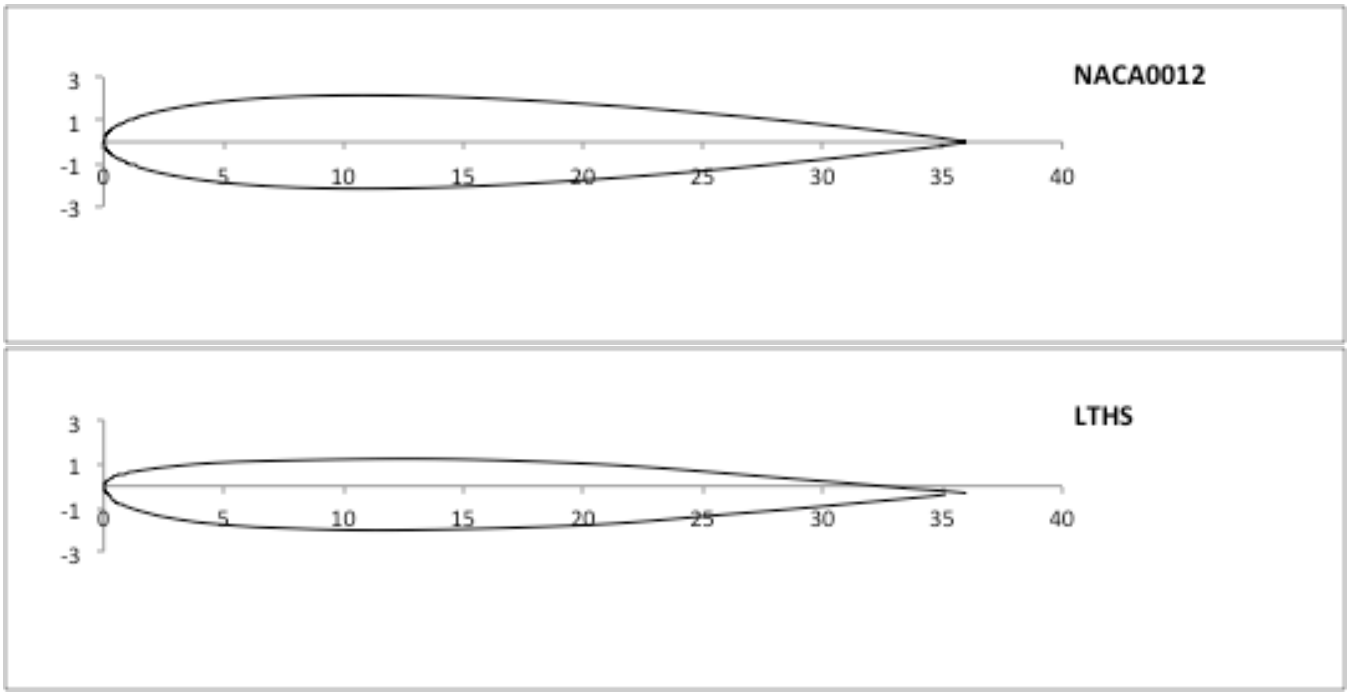

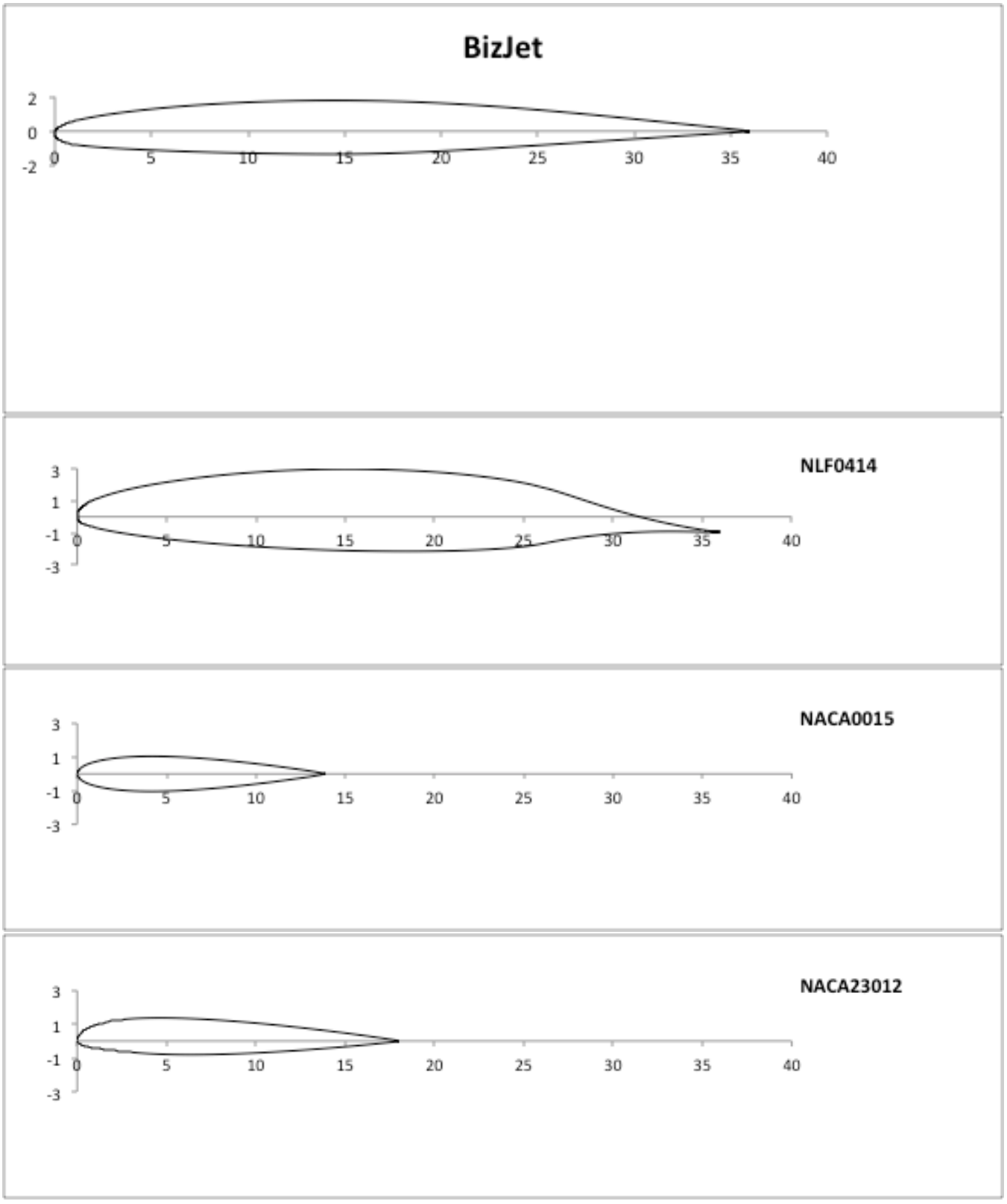

Figure 2: Airfoils Used in Validation Study

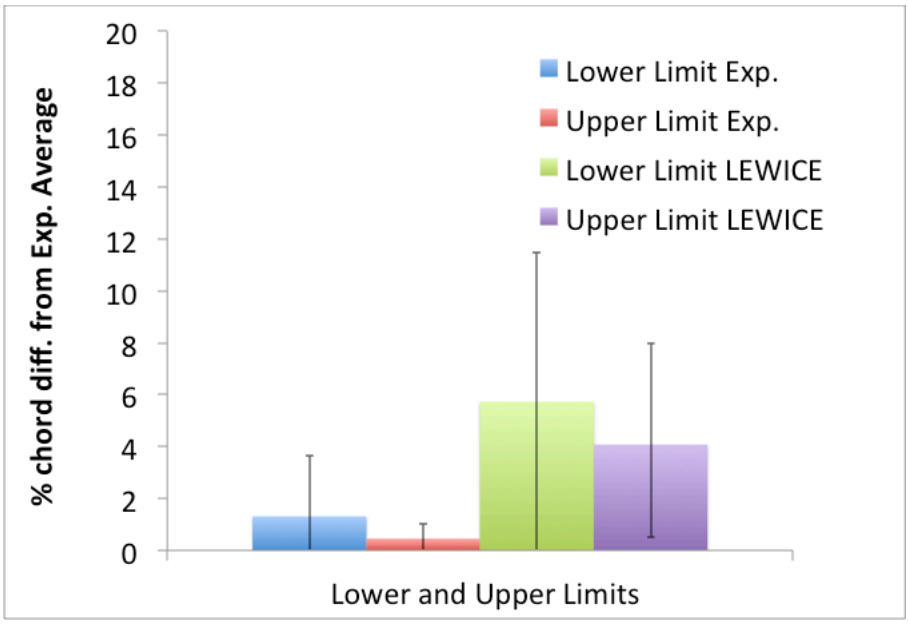

Figure 3: Comparison of Icing Limit Differences

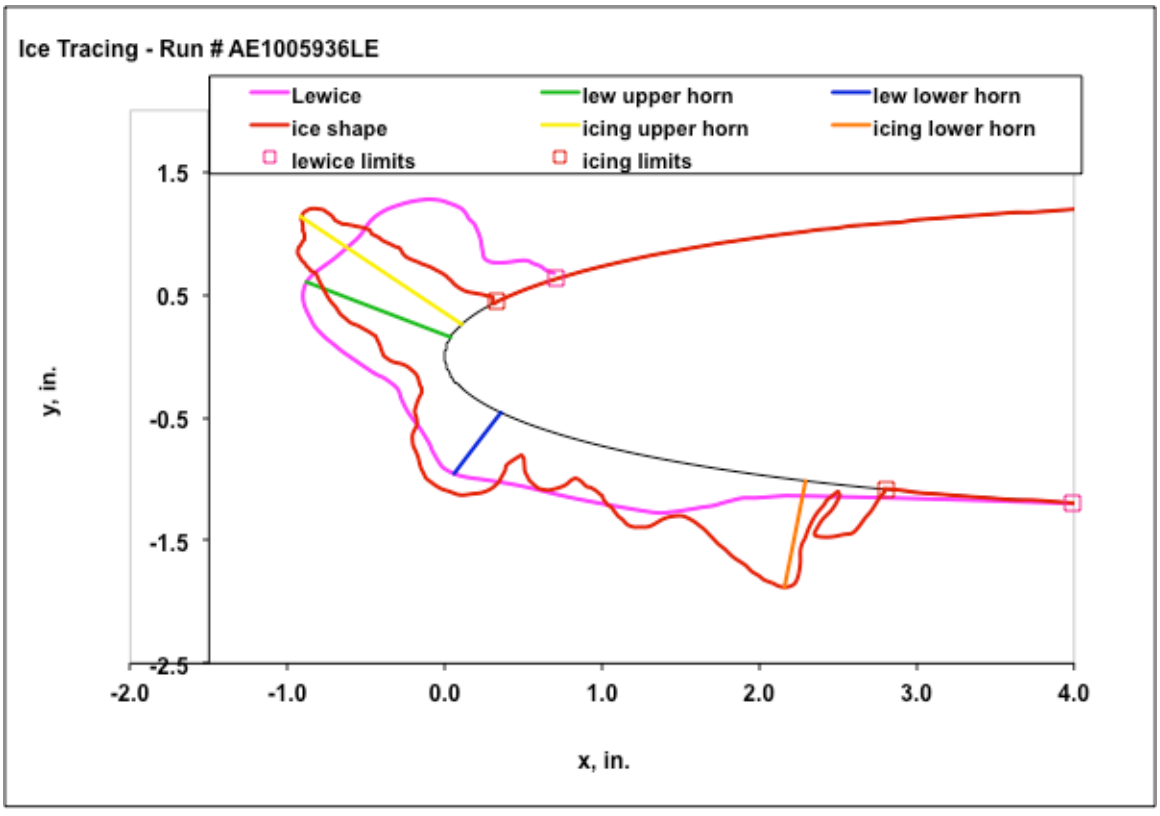

Figure 4: Ice Shape Comparison at Average Icing Limit

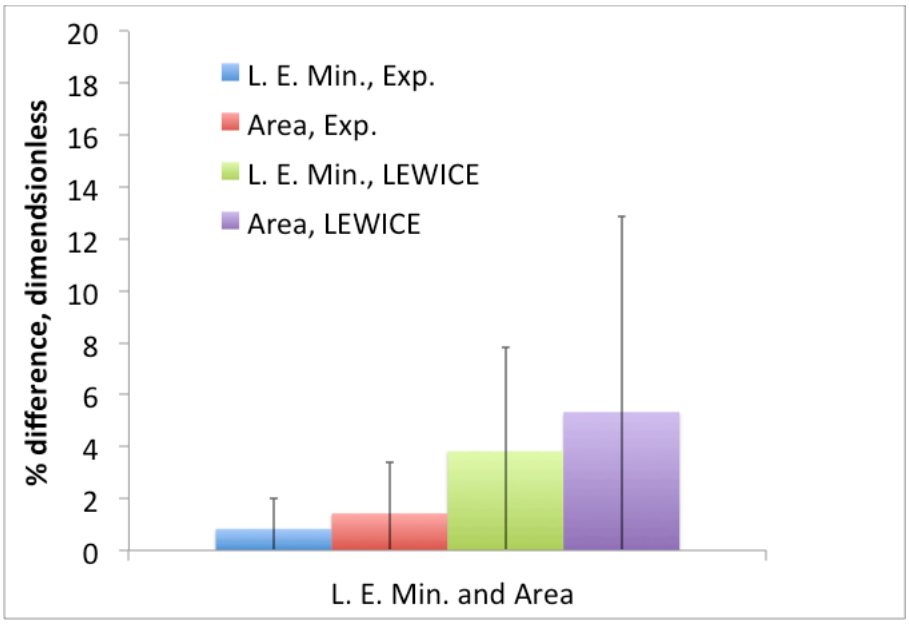

Figure 5: Comparison of Leading Edge Minimum and Area Differences

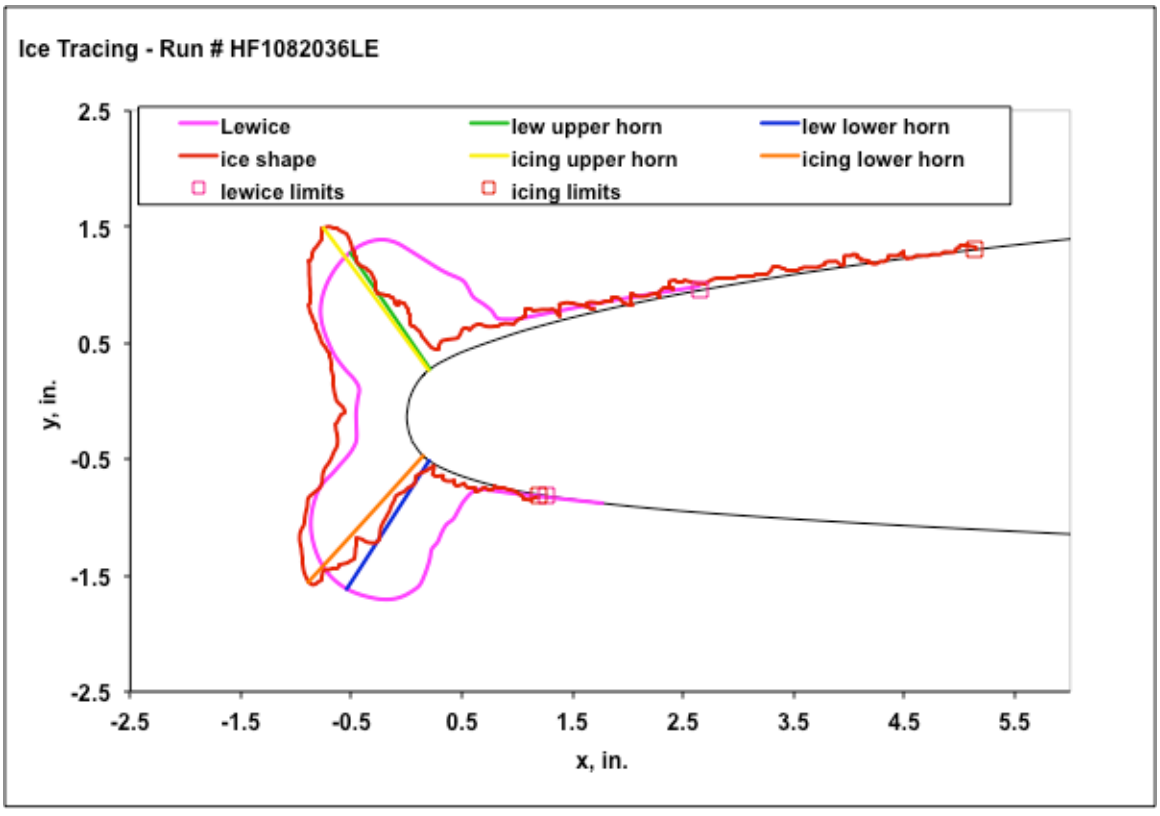

Figure 6: Ice Shape Comparison at Average Difference in Leading Edge Thickness and Area

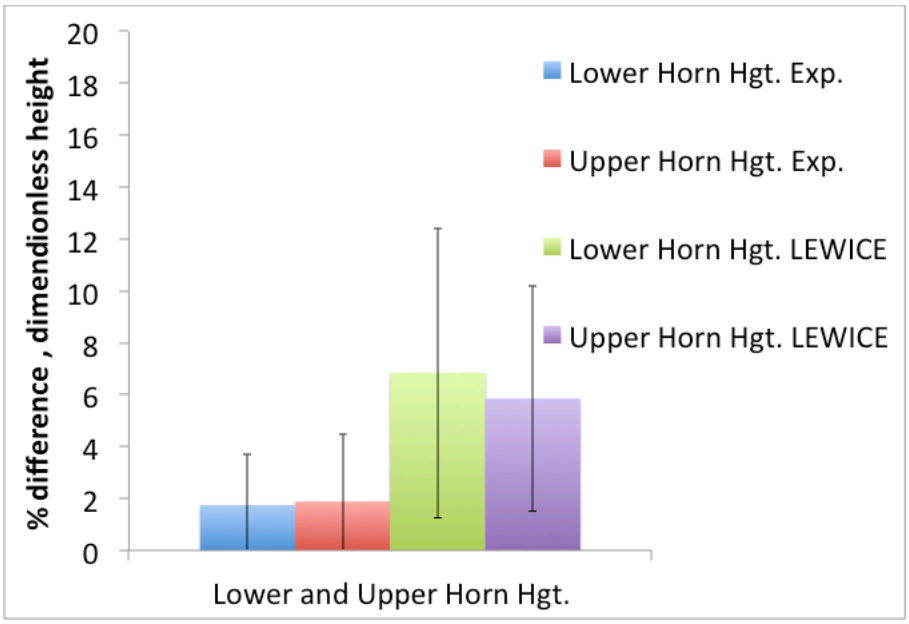

Figure 7: Comparison of Horn Height Differences

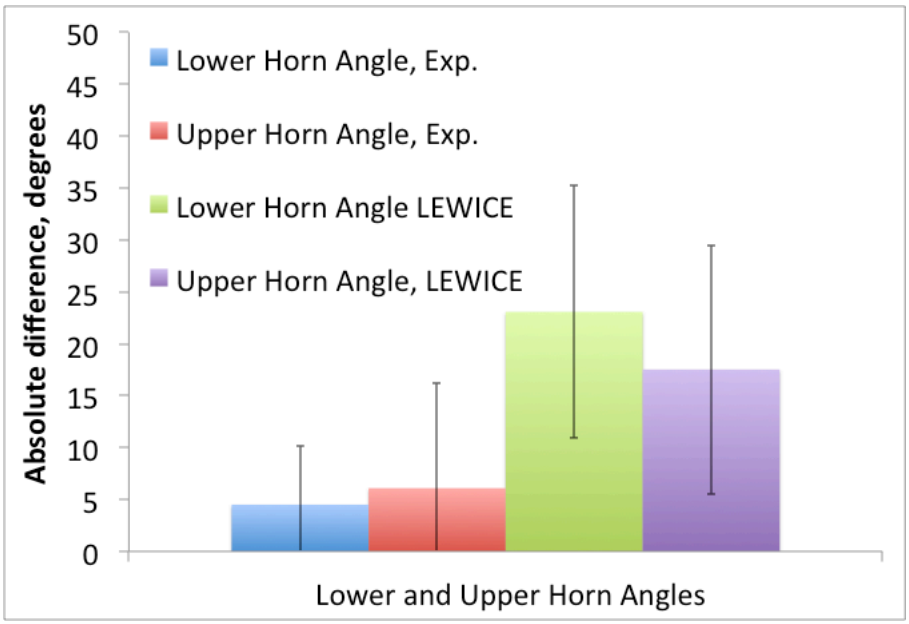

Figure 8: Comparison of Horn Angle Differences

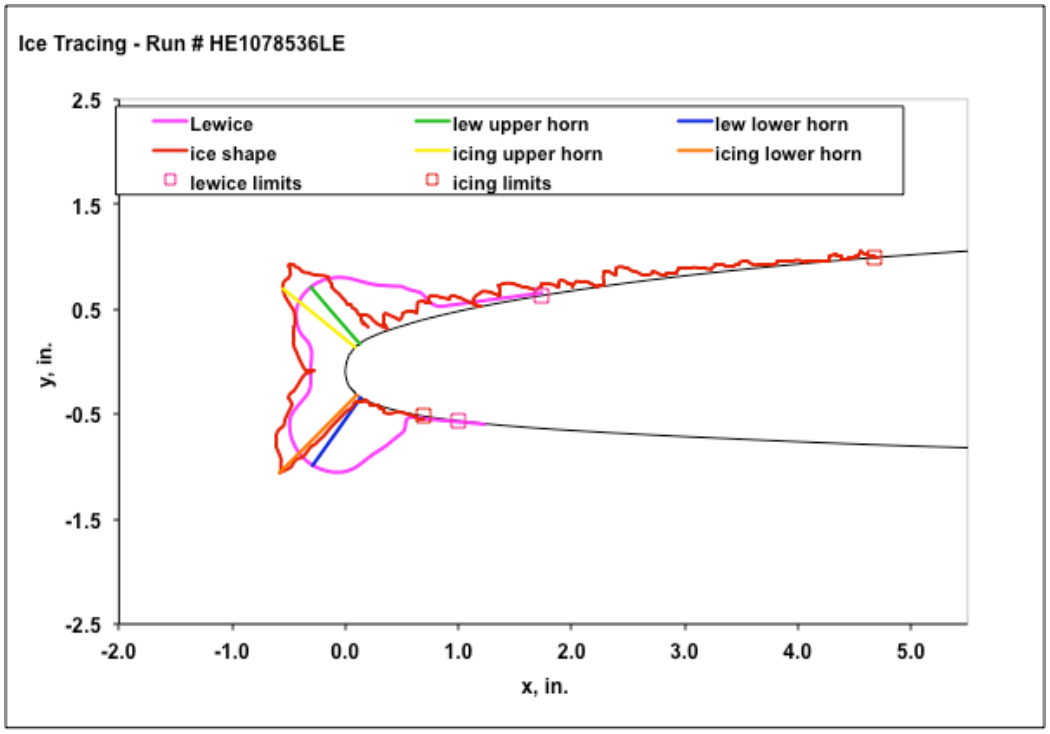

Figure 9: Ice Shape Comparison at Average Horn Height Differences

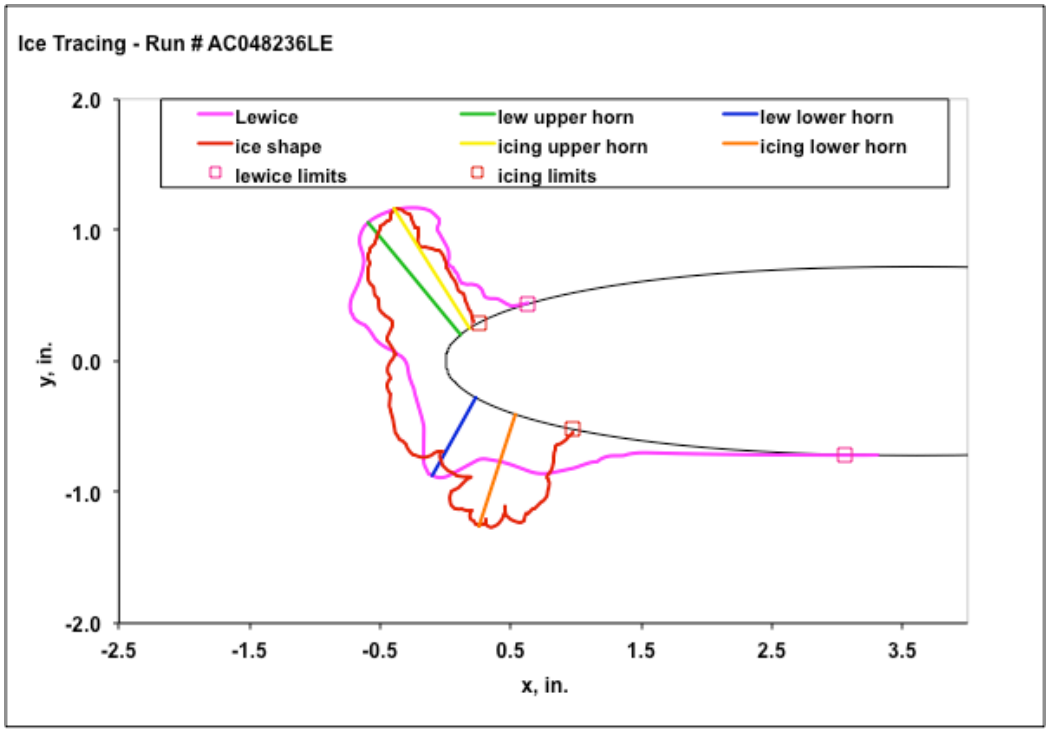

Figure 10: Ice Shape Comparison at Average Difference in Lower Horn Angle

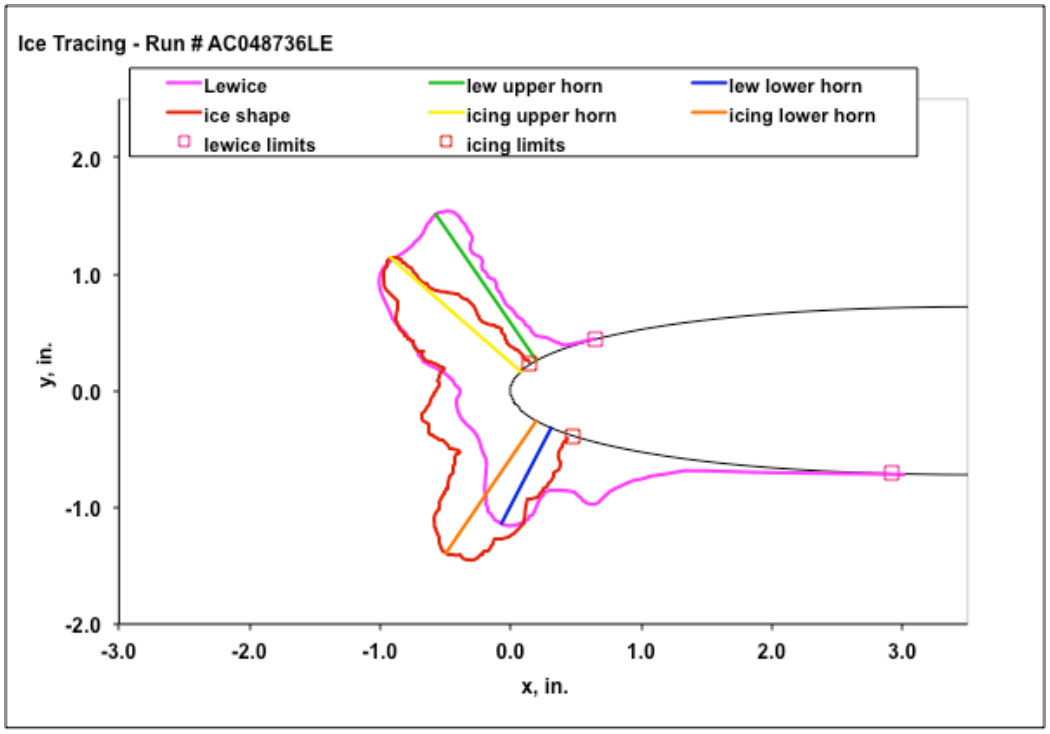

Figure 11: Ice Shape Comparison at Average Difference in Upper Horn Angle

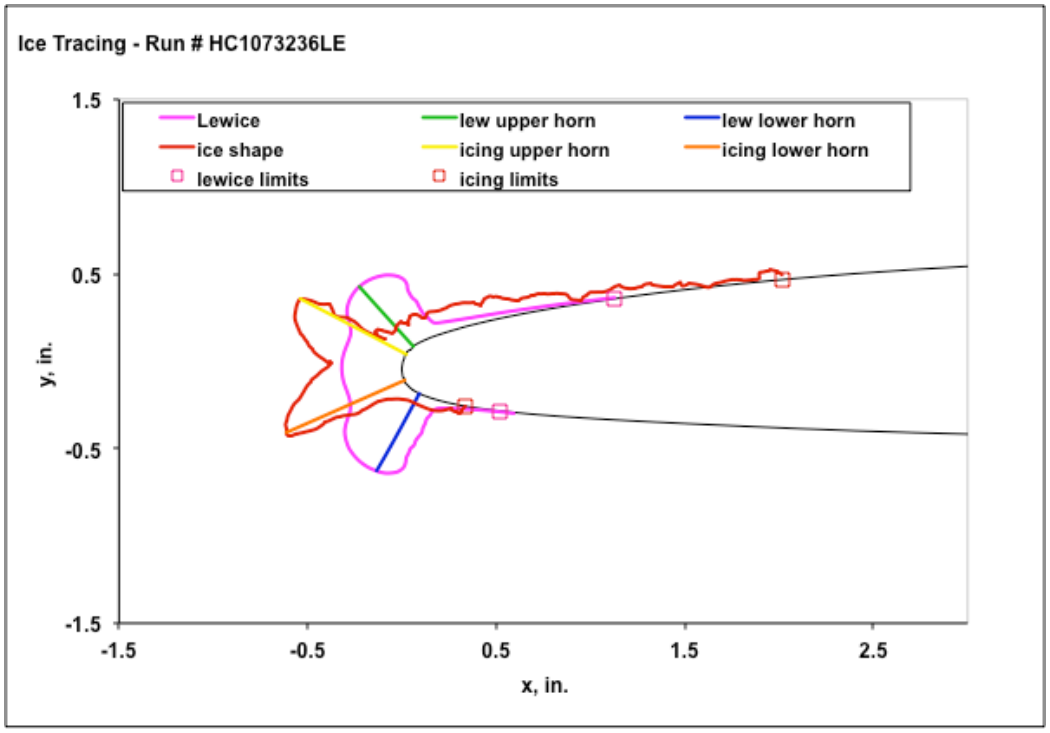

Figure 12: Worst LEWICE Comparison with Experiment, based on Lower Horn Angle

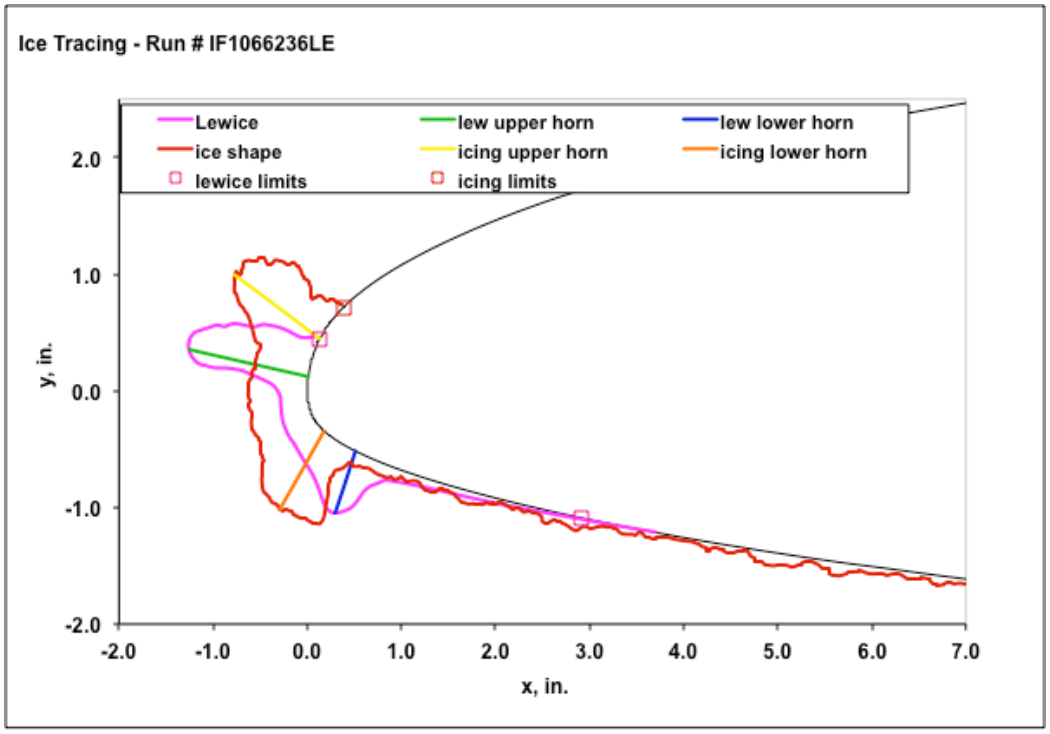

Figure 13: Worst LEWICE Comparison with Experiment, based on Upper Horn Angle

Table 1: Representative Lift and Drag Calculations

Case Name	Lift Coefficient	Lift Difference	Drag Coefficient	Drag Difference
HD1075736	0.5996	-0.0098	0.1280	0.0221
HD1075636	0.6205	0.0111	0.0824	-0.0235
HD1075936	0.6082	-0.0012	0.1074	0.0015
Average for this Condition	0.6094		0.1059	
LEWICE shape	0.6024	0.0070	0.1172	0.0113

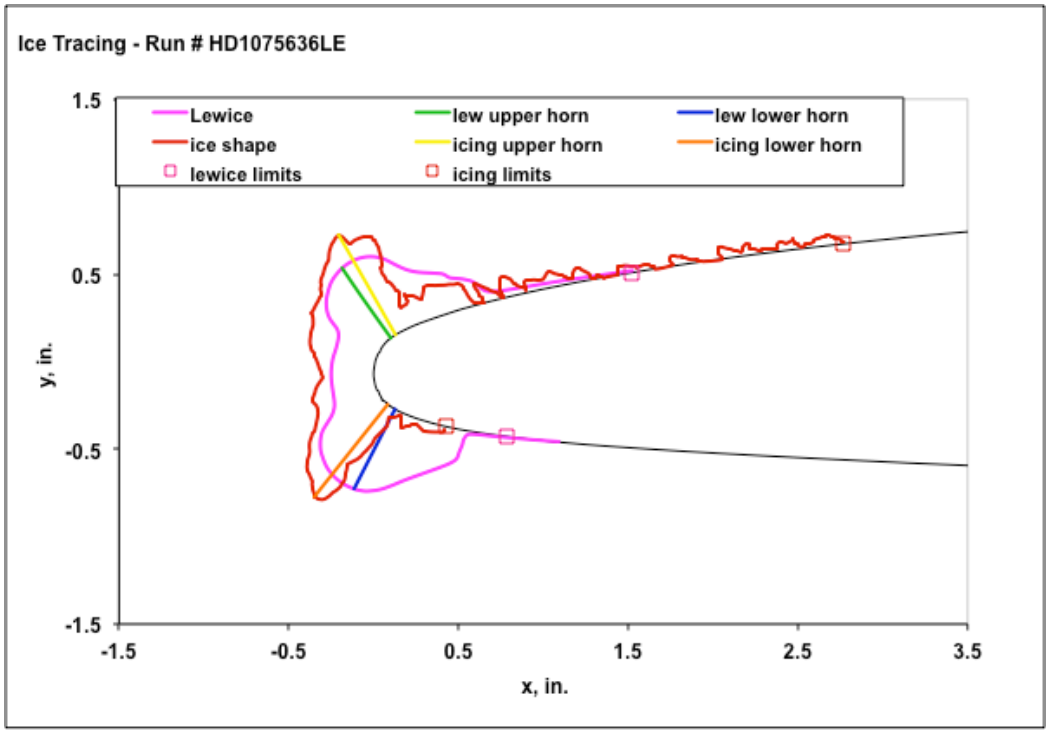

Figure 14: Ice Shape Prediction for HD1075636

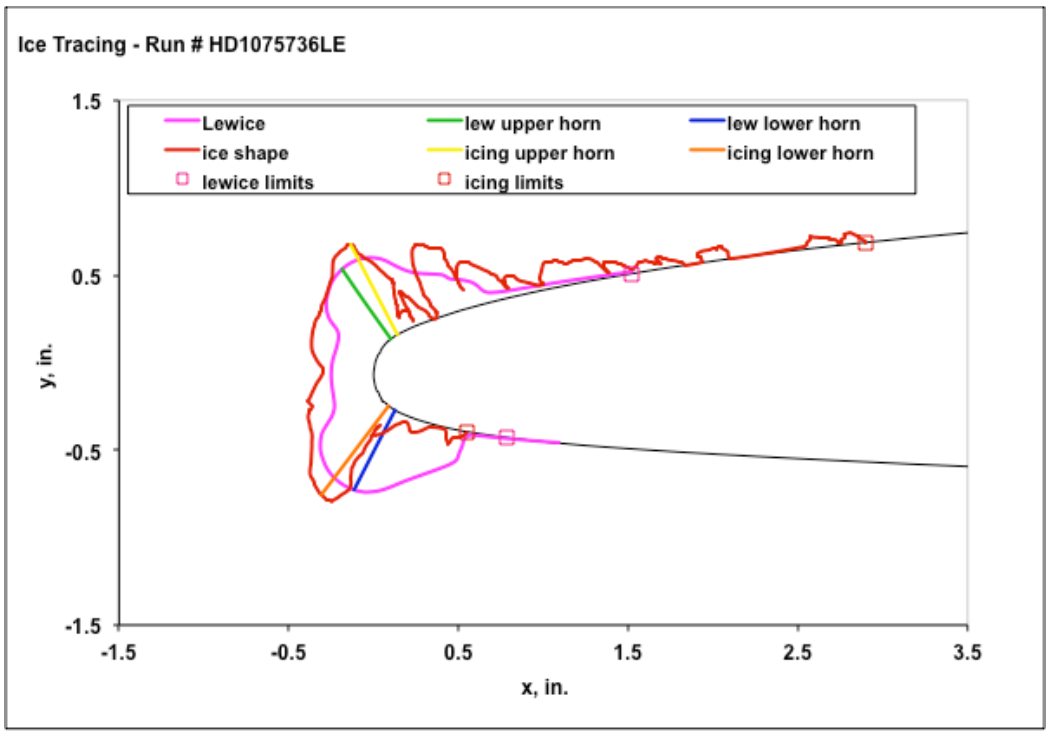

Figure 15: Ice Shape Prediction for HD1075736

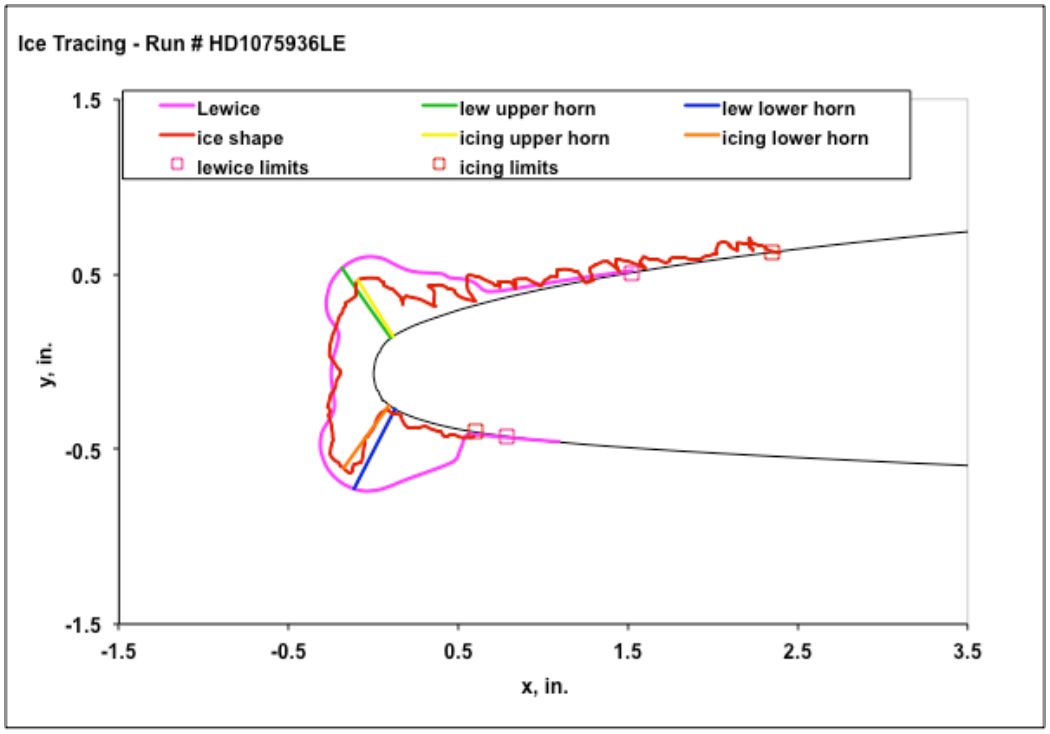

Figure 16: Ice Shape Prediction for HD1075936

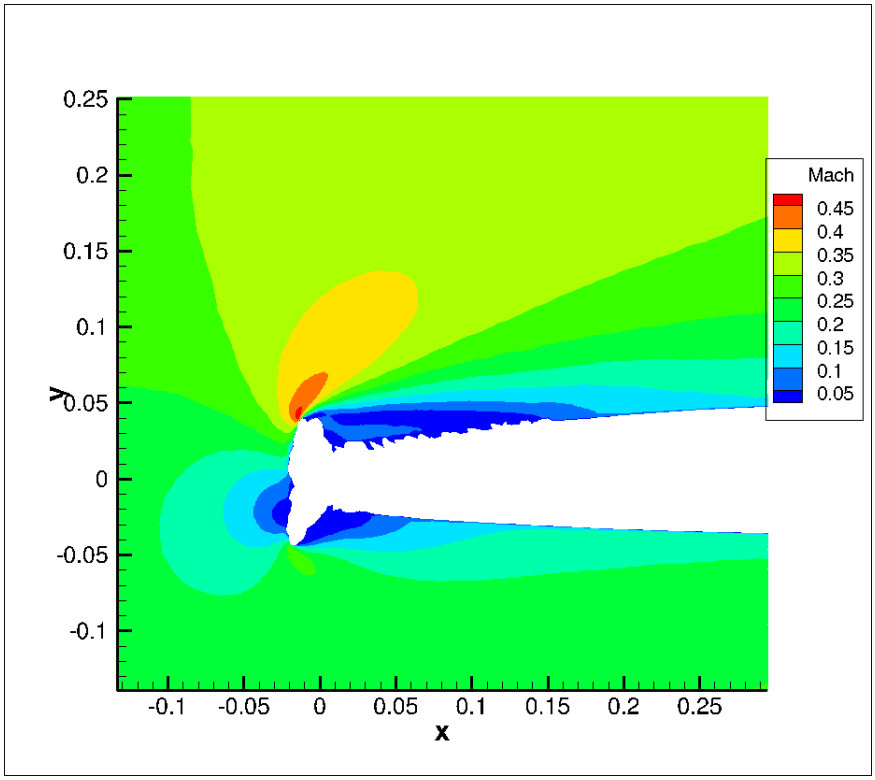

Figure 17: Mach Contours for HD1075636

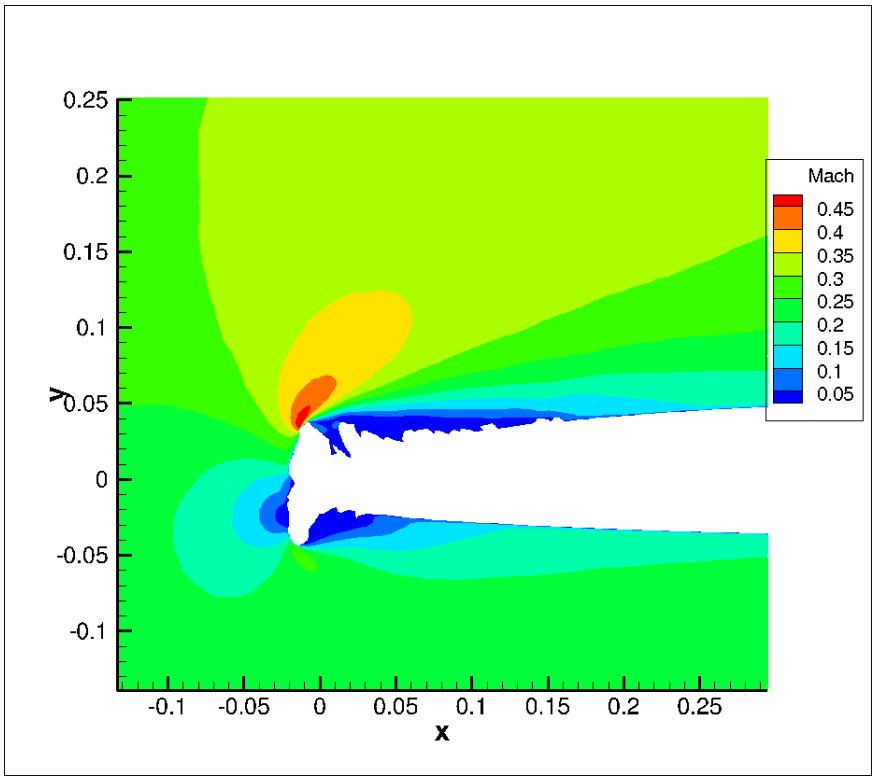

Figure 18: Mach Contours for HD1075736

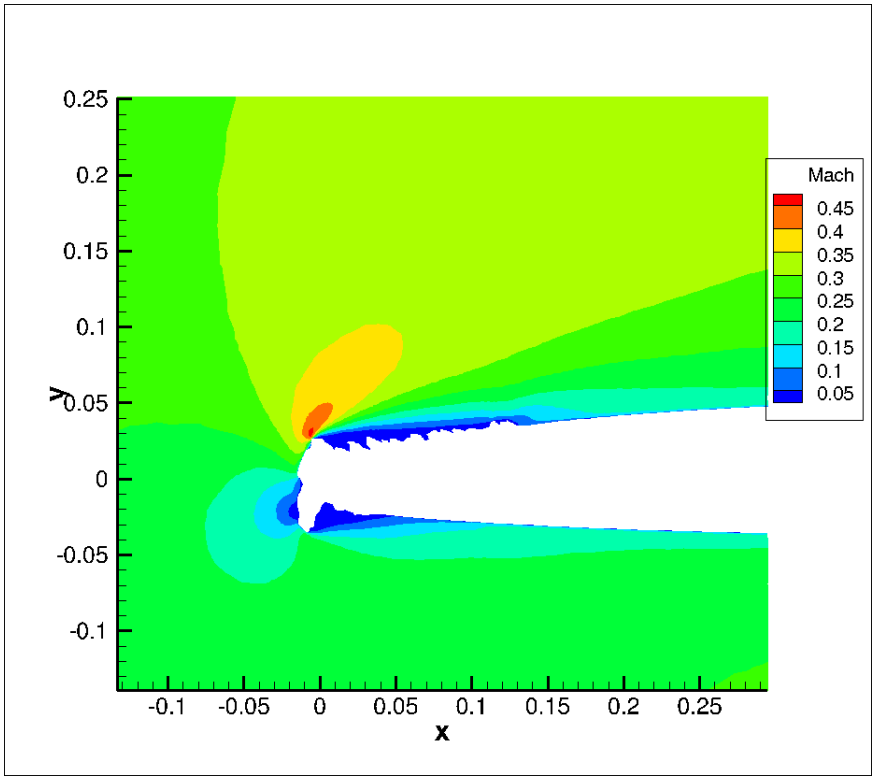

Figure 19: Mach Contours for HD1075936

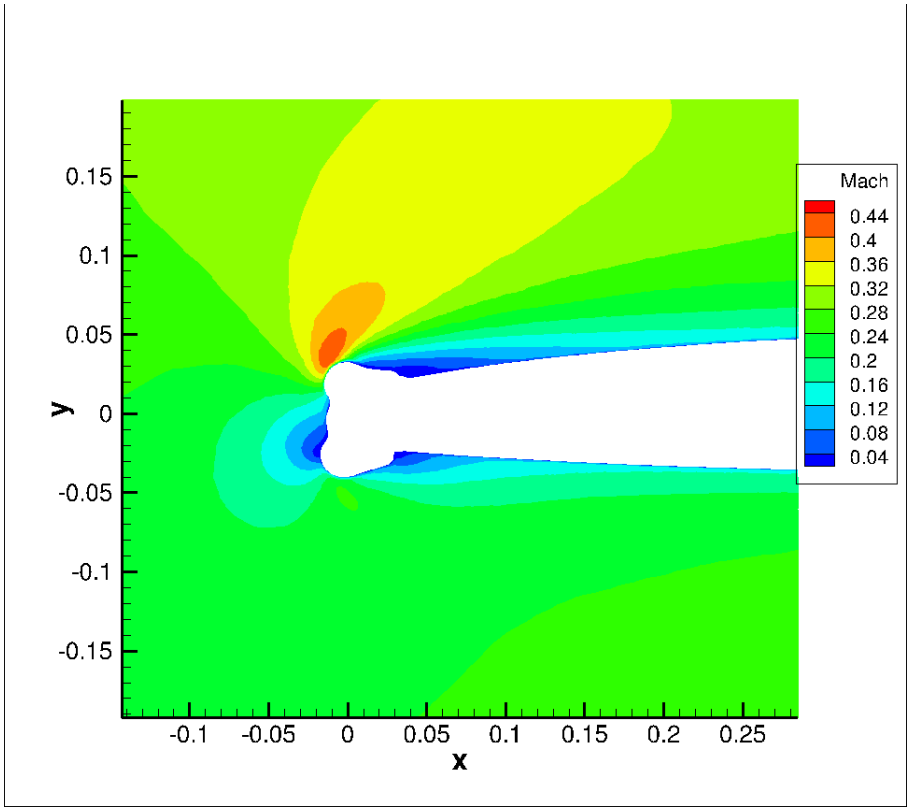

Figure 20: Mach Contours for LEWICE Shape Produced by HD1075636 Condition

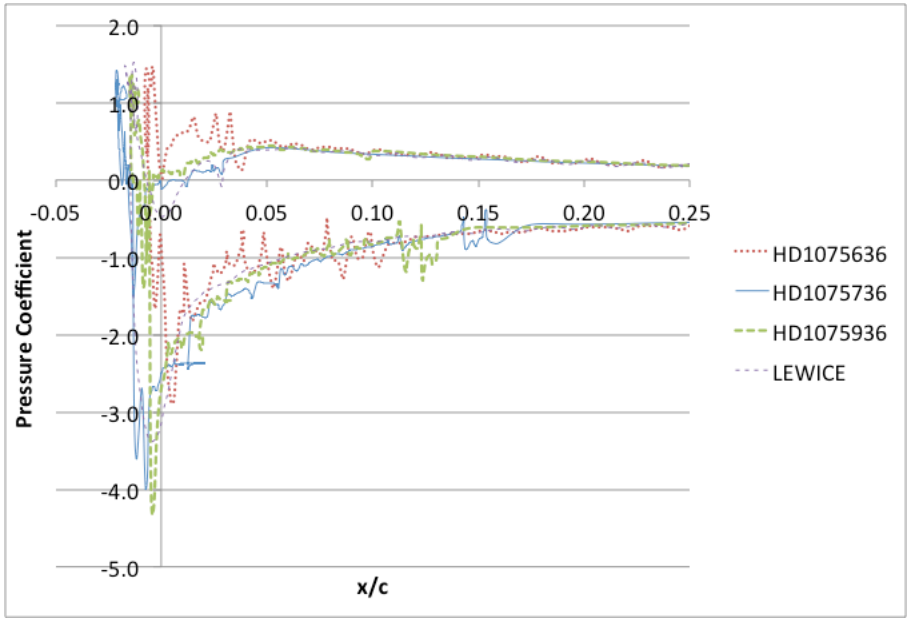

Figure 21: Pressure Coefficients for Sample Case HD1075636 and Repeats

Appendix A: List of Conditions

Case #	Reference Case Name	Airfoil	Chord (in)	Air Speed (kts)	AOA (deg)	Total Temp. (°F)	LWC (g/m^3)	MVD (μm)	Time (min)	Accum. Param. (by L.E. Dia.)
AC048230	AC048236	NACA0012	12.0	175.0	3.0	26.6	1.00	40.0	10.0	0.0250
AC048236	AC048236	NACA0012	12	175	3	26.6	1.00	40	10	0.0250
AC048242	AC048236	NACA0012	12.0	175.0	3.0	26.6	1.00	40.0	10.0	0.0250
AC048330	AC048336	NACA0012	12.0	175.0	3.0	26.6	0.50	20.0	15.0	0.0250
AC048336	AC048336	NACA0012	12	175	3	26.6	0.50	20	15	0.0250
AC048342	AC048336	NACA0012	12.0	175.0	3.0	26.6	0.50	20.0	15.0	0.0250
AC048430	AC048436	NACA0012	12.0	175.0	3.0	26.6	1.00	20.0	10.0	0.0500
AC048436	AC048436	NACA0012	12	175	3	26.6	1.00	20	10	0.0500
AC048442	AC048436	NACA0012	12.0	175.0	3.0	26.6	1.00	20.0	10.0	0.0500
AC048630	AC048636	NACA0012	12.0	132.0	3.0	23.4	1.00	20.0	15.0	0.0500
AC048636	AC048636	NACA0012	12	132	3	23.4	1.00	20	15	0.0500
AC048642	AC048636	NACA0012	12.0	132.0	3.0	23.4	1.00	20.0	15.0	0.0500
AC049930	AC048636	NACA0012	12.0	132.0	3.0	23.4	1.00	20.0	15.0	0.0500
AC049936	AC048636	NACA0012	12.0	132.0	3.0	23.4	1.00	20.0	15.0	0.0500
AC049942	AC048636	NACA0012	12.0	132.0	3.0	23.4	1.00	20.0	15.0	0.0500
AC048730	AC048736	NACA0012	12.0	132.0	3.0	23.4	1.00	40.0	15.0	0.0250
AC048736	AC048736	NACA0012	12	132	3	23.4	1.00	40	15	0.0250
AC048742	AC048736	NACA0012	12.0	132.0	3.0	23.4	1.00	40.0	15.0	0.0250
AC049830	AC048736	NACA0012	12.0	132.0	3.0	23.4	1.00	40.0	15.0	0.0250
AC049836	AC048736	NACA0012	12.0	132.0	3.0	23.4	1.00	40.0	15.0	0.0250
AC049842	AC048736	NACA0012	12.0	132.0	3.0	23.4	1.00	40.0	15.0	0.0250
AC1033636	AC1033636	NACA0012	10.5	115	0	22.0	1.04	37	8.96	0.0283
AC1036636	AC1036636	NACA0012	10.5	184	0	26.6	0.89	22	6.58	0.0408
AC1036836	AC1036836	NACA0012	10.5	168	0	25.9	0.75	23	8.56	0.0327
AC1037836	AC1037836	NACA0012	10.5	168	0	25.9	0.75	23	8.56	0.0327
AC1038136	AC1038136	NACA0012	10.5	125	0	22.4	1.22	35	7.05	0.0349
AC1038436	AC1038436	NACA0012	10.5	185	0	22.5	0.88	22	6.66	0.0404
AC1038936	AC1038936	NACA0012	10.5	185	0	22.1	0.75	19	7.8	0.0394
AC1040136	AC1040136	NACA0012	10.5	116	0	17.4	1.06	37	8.77	0.0289
AC1048736	AC1048736	NACA0012	10.5	185	0	22.5	0.88	22	6.66	0.0404
AC1049136	AC1049136	NACA0012	10.5	115	0	22.0	1.04	37	8.96	0.0283
AC1049336	AC1049336	NACA0012	10.5	167	0	21.2	0.78	23	8.27	0.0341
AC1049536	AC1049536	NACA0012	10.5	125	0	18.2	1.20	35	7.14	0.0343
AC1049736	AC1049736	NACA0012	10.5	116	0	17.4	1.06	37	8.77	0.0289
AC1050936	AC1050936	NACA0012	10.5	184	0	26.6	0.89	22	6.58	0.0408
AC1053036	AC1053036	NACA0012	10.5	167	0	21.2	0.78	23	8.27	0.0341
AD1046336	AD1046336	NACA0012	10.5	125	0	18.2	1.20	35	7.14	0.0343
AD1109236	AD1109236	NACA0012	14	200	0	19.5	0.61	175	13.8	0.0035
AD1109436	AD1109436	NACA0012	14	150	0	15.3	0.99	175	11.3	0.0057
AD1109836	AD1109836	NACA0012	14	100	0	12.4	1.68	175	10	0.0096
AE1005818	AE1005836	NACA0012	21.0	200.0	4.0	22.0	1.60	30.0	6.0	0.0533
AE1005824	AE1005836	NACA0012	21.0	200.0	4.0	22.0	1.60	30.0	6.0	0.0533
AE1005836	AE1005836	NACA0012	21	200	4	22.0	1.60	30	6	0.0533
AE1005854	AE1005836	NACA0012	21.0	200.0	4.0	22.0	1.60	30.0	6.0	0.0533
AE1006924	AE1005836	NACA0012	21.0	200.0	4.0	22.0	1.60	30.0	6.0	0.0533
AE1006936	AE1005836	NACA0012	21.0	200.0	4.0	22.0	1.60	30.0	6.0	0.0533
AE1006948	AE1005836	NACA0012	21.0	200.0	4.0	22.0	1.60	30.0	6.0	0.0533
AE1006954	AE1005836	NACA0012	21.0	200.0	4.0	22.0	1.60	30.0	6.0	0.0533
AE1005918	AE1005936	NACA0012	21.0	200.0	4.0	22.0	1.80	30.0	6.0	0.0600
AE1005924	AE1005936	NACA0012	21.0	200.0	4.0	22.0	1.80	30.0	6.0	0.0600
AE1005936	AE1005936	NACA0012	21	200	4	22.0	1.80	30	6	0.0600
AE1005954	AE1005936	NACA0012	21.0	200.0	4.0	22.0	1.80	30.0	6.0	0.0600
AE1006824	AE1005936	NACA0012	21.0	200.0	4.0	22.0	1.80	30.0	6.0	0.0600
AE1006836	AE1005936	NACA0012	21.0	200.0	4.0	22.0	1.80	30.0	6.0	0.0600

AE1006848	AE1005936	NACA0012	21.0	200.0	4.0	22.0	1.80	30.0	6.0	0.0600
AE1006854	AE1005936	NACA0012	21.0	200.0	4.0	22.0	1.80	30.0	6.0	0.0600
AE1111236	AE1111236	NACA0012	21	200	0	27.3	0.92	20	11.9	0.0460
AE1111336	AE1111236	NACA0012	21.0	200.0	0.0	27.4	0.92	20.0	11.9	0.0460
AE1111436	AE1111436	NACA0012	21	201	0	17.0	0.92	20	11.9	0.0460
AE1114636	AE1114636	NACA0012	21	200	0	22.1	1.03	20	11.9	0.0515
AE1114736	AE1114636	NACA0012	21.0	200.0	0.0	22.3	1.03	20.0	11.9	0.0515
AE1169736	AE1169736	NACA0012	21	200	0	20.0	0.70	20	15	0.0350
AE1169836	AE1169836	NACA0012	21	200	0	20.0	1.00	20	15	0.0500
AE1170136	AE1170136	NACA0012	21	70	0	20.0	1.70	20	15	0.0850
AE1170836	AE1170836	NACA0012	21	200	0	20.0	1.00	20	15	0.0500
AE1171136	AE1171136	NACA0012	21	200	0	20.0	0.80	20	10.3	0.0400
AE1171436	AE1171436	NACA0012	21	70	0	20.0	1.60	20	15	0.0800
AE1171936	AE1171936	NACA0012	21	200	0	20.0	0.80	20	15	0.0400
AE1172336	AE1172336	NACA0012	21	130	0	20.0	1.06	20	15	0.0530
AF080936	AF080936	NACA0012	36	200	1.5	23.0	0.83	29	20	0.0286
AF081536	AF081536	NACA0012	36	200	2.5	23.0	0.99	39	15	0.0254
AF081636	AF081636	NACA0012	36	200	2.5	23.0	0.96	37	15	0.0262
AF084236	AF084236	NACA0012	36	200	2.5	23.0	0.98	26	15	0.0378
AF1161336	AF1161336	NACA0012	36	150	0	22.8	1.15	20	17	0.0575
	AF1160636	NACA0012	36	100	0	17.6	1.14	20	28.1	0.0570
AF1181736	AF1181736	NACA0012	36	100	0	19.1	1.10	15	31.9	0.0733
AF1182436	AF1181736	NACA0012	36.0	100.0	0.0	19.1	1.10	15.0	31.9	0.0733
AF1181836	AF1181836	NACA0012	36	150	0	17.0	1.00	15	20.4	0.0667
AF1182536	AF1181836	NACA0012	36.0	149.9	0.0	17.0	1.00	15.0	20.4	0.0667
AF1195036	AF1195036	NACA0012	36.0	100.0	0.0	26.2	0.50	15.0	69.7	0.0333
AF1195436	AF1195436	NACA0012	36.0	100.0	0.0	20.2	1.00	15.0	34.8	0.0667
AF1195136	AF1195136	NACA0012	36	100	0	25.6	1.00	15	34.87	0.0667
ED071136	ED071136	NACA23012	18	250	2	20.0	0.67	15	10	0.0435
ED071230	ED071230	NACA23012	18	250	2	24.0	0.67	15	10	0.0435
HC1070636	HC1070636	BizJet	12	271	0	28.8	1.13	19	2.3	0.0595
HC1070736	HC1070636	BizJet	12.0	270.9	0.0	28.8	1.13	19.0	2.3	0.0595
HC1071036	HC1071036	BizJet	12	290	0	29.6	1.15	20	2.1	0.0575
HC1071136	HC1071036	BizJet	12.0	289.6	0.0	29.6	1.15	20.0	2.1	0.0575
HC1071536	HC1071536	BizJet	12	170	0	21.2	1.62	23	2.3	0.0695
HC1072436	HC1072436	BizJet	12	271	0	17.7	1.12	19	2.3	0.0589
HC1072536	HC1072436	BizJet	12.0	271.0	0.0	17.7	1.12	19.0	2.3	0.0589
HC1072836	HC1072836	BizJet	12	292	0	18.4	1.12	19	2.1	0.0589
HC1072936	HC1072836	BizJet	12.0	292.3	0.0	18.4	1.12	19.0	2.1	0.0589
HC1073236	HC1073236	BizJet	12	170	0	8.5	1.80	23	2.3	0.0783
HC1073336	HC1073236	BizJet	12.0	169.9	0.0	8.5	1.80	23.0	2.3	0.0783
HD1074836	HD1074836	BizJet	18	220	0	22.3	1.50	26	3.1	0.0577
HD1074936	HD1074836	BizJet	18.0	220.2	0.0	22.3	1.50	26.0	3.1	0.0577
HD1075236	HD1075236	BizJet	18	206	0	21.9	1.49	27	3.3	0.0552
HD1075336	HD1075236	BizJet	18.0	205.6	0.0	21.9	1.49	27.0	3.3	0.0552
HD1075636	HD1075636	BizJet	18	172	0	21.1	1.47	29	4	0.0507
HD1075736	HD1075636	BizJet	18.0	171.9	0.0	21.1	1.47	29.0	4.0	0.0507
HD1075836	HD1075636	BizJet	18.0	171.9	0.0	21.1	1.47	29.0	4.0	0.0507
HD1075936	HD1075636	BizJet	18.0	171.9	0.0	21.1	1.47	29.0	4.0	0.0507
HD1076036	HD1076036	BizJet	18	217	0	9.5	1.42	27	3.3	0.0526
HD1076436	HD1076436	BizJet	18	207	0	9.2	1.42	27	3.44	0.0526
HD1076736	HD1076736	BizJet	18	172	0	8.5	1.47	29	4	0.0507
HE1077536	HE1077536	BizJet	24	155	0	24.3	0.81	31	10.1	0.0264
HE1078236	HE1078236	BizJet	24	174	0	21.3	1.20	36	6.1	0.0331
HE1078336	HE1078236	BizJet	24.0	173.4	0.0	21.4	1.20	36.2	6.1	0.0332
HE1078436	HE1078436	BizJet	24	172	0	21.4	1.31	20	6.1	0.0652
HE1078536	HE1078536	BizJet	24	174	0	21.2	1.30	35	6	0.0371
HE1078636	HE1078536	BizJet	24.0	173.7	0.0	21.2	1.30	35.0	6.0	0.0371
HE1079136	HE1079136	BizJet	24	174	0	8.6	1.30	35	6	0.0371

HE1079236	HE1079136	BizJet	24.0	173.7	0.0	8.6	1.30	35.0	6.0	0.0371
HE1079736	HE1079736	BizJet	24	159	0	14.2	0.93	36	9.2	0.0258
HE1079836	HE1079736	BizJet	24.0	159.0	0.0	14.2	0.93	36.0	9.2	0.0258
HE1079936	HE1079936	BizJet	24	191	0	2.3	1.87	34	3.8	0.0550
HE1080036	HE1080036	BizJet	24	187	0	14.3	0.92	34	7.8	0.0271
HE1080136	HE1080136	BizJet	24	159	0	1.4	1.96	36	4.4	0.0544
HE1080236	HE1080236	BizJet	24	171	0	14.2	0.93	35	8.5	0.0266
HE1080336	HE1080336	BizJet	24	177	0	1.8	1.91	35	4	0.0546
HE1080536	HE1080536	BizJet	24	174	0	8.6	1.27	43	6	0.0295
HE1080736	HE1080536	BizJet	24.0	173.7	0.0	8.6	1.27	43.0	6.0	0.0295
HE1080636	HE1080636	BizJet	24	174	0	8.8	1.20	36	6.1	0.0331
HE1080836	HE1080836	BizJet	24	173	0	8.9	1.30	20	6.1	0.0647
HF1009536	HF1009536	BizJet	36	175	6	30.6	0.54	20	22.5	0.0270
HF1014436	HF1009536	BizJet	36	175	6	30.6	0.54	20	22.4	0.0270
HF1026930	HF1009536	BizJet	36.0	175.0	6.0	30.6	0.54	20.0	22.5	0.0270
HF1026936	HF1009536	BizJet	36	175	6	30.6	0.54	20	22.5	0.0270
HF1026942	HF1009536	BizJet	36.0	175.0	6.0	30.6	0.54	20.0	22.5	0.0270
HF1009636	HF1009636	BizJet	36	175	6	30.6	0.54	20	45	0.0270
HF1009936	HF1009936	BizJet	36	175	6	28.9	0.41	20	33.3	0.0205
HF1010436	HF1010436	BizJet	36	175	6	21.4	0.60	15	22.5	0.0400
HF1010536	HF1010536	BizJet	36	175	6	21.2	0.60	15	45	0.0400
HF1012936	HF1012936	BizJet	36	175	4	30.6	0.54	20	22.5	0.0270
HF1013136	HF1013136	BizJet	36	212	4	24.9	0.43	20	22.5	0.0215
HF1013236	HF1013236	BizJet	36	175	4	31.0	0.54	20	22.5	0.0270
HF1013636	HF1013636	BizJet	36	175	6	24.2	1.60	20	8.4	0.0800
HF1013936	HF1013936	BizJet	36	175	6	12.3	1.60	20	8.4	0.0800
HF1014236	HF1014236	BizJet	36	175	4	12.3	0.83	160	20	0.0052
HF1014336	HF1014336	BizJet	36	175	6	30.6	0.83	160	20	0.0052
HF1081736	HF1081736	BizJet	36	128	0	20.2	1.15	50	13.8	0.0230
HF1082036	HF1082036	BizJet	36	137	0	20.7	1.10	50	13.5	0.0220
HF1082136	HF1082036	BizJet	36.0	137.2	0.0	20.7	1.10	50.0	13.5	0.0220
HF1082436	HF1082436	BizJet	36	176	0	21.2	1.11	45	10.4	0.0247
HF1082536	HF1082436	BizJet	36.0	176.3	0.0	21.2	1.11	45.0	10.4	0.0247
HF1082836	HF1082836	BizJet	36	129	0	8.1	1.17	50	13.4	0.0234
HF1083136	HF1083136	BizJet	36	136	0	8.1	1.16	50	12.9	0.0232
HF1083436	HF1083436	BizJet	36	176	0	8.6	1.10	45	10.5	0.0244
IF1066230	IF1066236	NLF0414	36.0	130.0	2.0	26.4	0.54	20.0	22.5	0.0270
IF1066236	IF1066236	NLF0414	36.0	130.0	2.0	26.4	0.54	20.0	22.5	0.0270
IF1066242	IF1066236	NLF0414	36.0	130.0	2.0	26.4	0.54	20.0	22.5	0.0270
IF1066330	IF1066236	NLF0414	36.0	130.0	2.0	26.4	0.54	20.0	22.5	0.0270
IF1069130	IF1069136	NLF0414	36.0	130.0	0.0	28.2	1.00	20.5	15.0	0.0488
IF1069136	IF1069136	NLF0414	36.0	130.0	0.0	28.2	1.00	20.5	15.0	0.0488
IG1059742	IG1059742	NLF0414	48.4	135	1	24.0	0.70	20	45	0.0350
JF1024130	JF1024136	LTHS	36.0	250.0	0.0	32.0	0.41	20.0	22.5	0.0205
JF1024136	JF1024136	LTHS	36	250	0	32.0	0.41	20	22.5	0.0205
JF1024142	JF1024136	LTHS	36.0	250.0	0.0	32.0	0.41	20.0	22.5	0.0205
JF1025436	JF1025436	LTHS	36	253	-1	29.5	0.56	21	18.5	0.0267
JF1025630	JF1025636	LTHS	36.0	253.0	0.0	29.5	0.56	21.0	36.9	0.0268
JF1025636	JF1025636	LTHS	36	253	0	29.5	0.56	21	36.9	0.0267
JF1025730	JF1025736	LTHS	36.0	253.0	0.0	29.5	0.56	21.0	24.6	0.0268
JF1025736	JF1025736	LTHS	36	253	0	29.5	0.56	21	24.6	0.0267
JF1025742	JF1025736	LTHS	36.0	253.0	0.0	29.5	0.56	21.0	24.6	0.0268
JF1025830	JF1025830	LTHS	36	253	0	29.5	0.56	21	18.5	0.0267
OD1057336	OD1057336	NACA0015	13.9	185	0	31.1	0.75	19	10	0.0395
OD1057436	OD1057436	NACA0015	13.9	166	0	29.9	0.68	23	12.2	0.0291
OD1057536	OD1057536	NACA0015	13.9	185	0	22.1	0.75	19	10	0.0395
OD1057636	OD1057536	NACA0015	13.9	185.1	0	22.1	0.75	19	10	0.0395
OD1057836	OD1057836	NACA0015	13.9	166	0	20.9	0.77	23	10.8	0.0329